Numerical Analysis of Aerodynamic Performance of a Fixed-Pitch Vertical Axis Wind Turbine Rotor

Rogowski, Krzysztof; Michna, Jan; Ferreira, Carlos

DOI
10.12913/22998624/191128

Publication date
2024

Document Version
Final published version

Published in
Advances in Science and Technology Research Journal

Citation (APA)
Rogowski, K., Michna, J., & Ferreira, C. (2024). Numerical Analysis of Aerodynamic Performance of a Fixed-Pitch Vertical Axis Wind Turbine Rotor. *Advances in Science and Technology Research Journal*, *18*(6), 97-109. https://doi.org/10.12913/22998624/191128

Advances in Science and Technology Research Journal

Advances in Science and Technology Research Journal, 18(6), 97–109
https://doi.org/10.12913/22998624/191128
ISSN 2299-8624, License CC-BY 4.0

Received: 2024.06.10
Accepted: 2024.08.15
Published: 2024.09.08

Numerical Analysis of Aerodynamic Performance of a Fixed-Pitch Vertical Axis Wind Turbine Rotor

Krzysztof Rogowski[1*], Jan Michna[1], Carlos Ferreira[2]

[1] Institute of Aeronautics and Applied Mechanics, Warsaw University of Technology, Nowowiejska 24, 00-665 Warsaw, Poland

[2] Faculty of Aerospace Engineering, Delft University of Technology, Kluyverweg 1, 2629 HS Delft, The Netherlands

* Corresponding author's e-mail: krzysztof.rogowski@pw.edu.pl

ABSTRACT

The aim of this study was to assess the accuracy of predicting the aerodynamic loads and investigate the aerodynamic wake characteristics of a vertical axis wind turbine (VAWT) rotor using a simplified two-dimensional numerical rotor model and an advanced numerical approach – the Scale Adaptive Simulation (SAS) coupled with the four-equation $\gamma - Re_{\theta}$ turbulence model. The challenge for this approach lies in the operating conditions of the rotor, the blade pitch angles, and the very small geometric dimensions of the rotor. The rotor, with a diameter of 0.3 m, operates at a low tip speed ratio of 2.5 and an extremely low blade Reynolds number of approximately 22.000, whereas the pitch angles, β, are: -10, 0, and 10 degrees. Validation was conducted based on high-fidelity measurements obtained using the PIV technique at TU Delft. The obtained results of rotor loads and velocity profiles are surprisingly reliable for cases of $\beta = 0°$ and $\beta = –10°$. However, the 2-D model is too imprecise to estimate both aerodynamic loads and velocity fields accurately.

Keywords: wind turbine, VAWT, Darrieus, aerodynamics, RANS, scale adaptive simulation, turbulence.

INTRODUCTION

As the global discussion about the consequences of exploiting fossil fuels grows, the development of green energy sources has increased widely. In the wind energy industry, the concerns have been focused mainly on horizontal-axis wind turbines (HAWTs) since the 1970s and the fuel crisis. This type of turbine is well-investigated, and improving its aerodynamic performance is challenging. More and more efforts are concentrated on vertical-axis wind turbines (VAWTs), especially to bridge the aerodynamic performance gap between these two types [1, 2].

VAWT has many advantages over the horizontal-axis type. It does not need any yaw mechanics, a smaller wake area behind the rotor, and low installation and maintenance costs because of easy access to the generator lying on the ground [3]. However, the vertical-axis type poses some challenges, e.g., complex turbine aerodynamics, a demanding self-starting process (low self-start torque), and generally lower current efficiency than HAWTs.

The most critical challenge is rotor aerodynamic performance estimation because of the phenomena which are complicated to model, such as dynamic stall and blade-wake interaction [4]. The power performance of VAWTs depends on various operational parameters, among others, an airfoil (shape, chord length), blade pitch angle, the solidity of a turbine, Reynolds numbers, tip speed ratio, shaft diameter, and turbulence intensity [1, 5].

To study blade pitch angle, one of the operational parameters, many researchers investigated the power performance of fixed- and variable-pitch angle VAWT. Fiedler and Tullis [6] found that toe-in fixed pitch angle can significantly

lower the wind turbine performance. Using large eddy simulations (LES) with experimental measurements, Elkhoury et al. [7] demonstrated that variable-pitch mechanisms can give higher power coefficients than fixed-pitch ones. Rezaieha et al. [8] showed a large hysteresis of dynamic loads on the blades and boundary layer events (such as laminar-to-turbulent transition). Meanwhile, Huang et al. [9] proved that pitch angle configuration significantly influences wake deflection and deformation. Szczerba et al. [10] noticed that achieving the best performance requires high blade setting precision with less than 1 degree tolerance. Elsakka et al. [11] demonstrated that pitch angle has a lower influence on power performance than tip speed ratio and solidity, but switching angle improves turbine aerodynamic performance.

In the presented research, the well-known γ–Re_θ transition turbulence model was utulized [12]. This four-equation model includes the intermittency and transition momentum thickness transport equations, combined with the two-equation k-ω SST turbulence model. This correlation-based approach was designed for general-purpose use across a broad range of flow classes, but as a correlation model, it requires validation against experimental data or high-fidelity simulations such as LES or detached eddy simulation (DES) [13]. The complex flow at the very low Reynolds number of approximately 22.000 considered in this study presents significant validation challenges due to the scarcity of experimental data. ANSYS Fluent provides two transition models, γ–Re_θ and κ–κ_L–ω, both of which necessitate validation and calibration based on experimental studies to ensure accurate predictions.

VERTICAL AXIS WIND TURBINE AND ITS OPERATIONAL CONDITIONS

This study analyzed a simplified two-dimensional model of a vertical-axis wind turbine (VAWT) rotor. The rotor consists of only two symmetrical NACA0012 airfoils representing blades of infinite length. Additional simplifications of the model include the lack of a rotating shaft and blade supports (e.g., struts). The geometric dimensions of the rotor, such as the rotor diameter (D = 0.3 m) and the airfoil chord length (c = 0.03 m), correspond to the dimensions of a wind turbine developed by TU Delft for laboratory-scale research. The attachment point of the blade was located at one-quarter of the chord length measured from the airfoil leading edge. The study analyzed the rotor performance for three fixed blade pitch angles, β, (the blade pitch angle remained constant during rotor's movement). Figure 1 shows the simplified wind turbine model and the convention for indicating the sign of blade pitch angles. Positive pitch angles mean the blade is turned inward.

The operational parameters of the rotor are as follows: the undisturbed flow velocity, V_0, is 5 m/s; rotor rotational velocity is assumed to be 800 rpm; tip speed ratio, *TSR*, is equal to 2.5. The tip speed ratio is a dimensionless quantity that relates the angular velocity ω of the rotor, its radius, R, and the velocity of the undisturbed flow: $TSR = \omega \cdot R/V_0$. Figure 1 depicts the velocity vectors and illustrates the method of measuring rotor position using the azimuthal angle θ. A schematic of the laboratory-scale VAWT model is additionally presented in Figure 1. During the wind tunnel tests, two components of the aerodynamic force were measured using three load cells mounted on the bottom of the standing frame. Details of the experiment can be found in [14].

GRID AND COMPUTATIONAL METHODOLOGY

This paper section first describes the computational domain and the numerical grid used for the calculations. The numerical model settings are described in the subsequent part of this section.

The two-bladed wind turbine rotor was surrounded by a rectangular domain with dimensions of 7.5 × 6 m, corresponding to 25 × 20 D, where D represents the rotor diameter (Fig. 2). These dimensions were selected based on the numerical study by Rezaeiha et al. [15], who analyzed the impact of domain size and the distance of the rotor axis from the inlet on the aerodynamic performance of the wind turbine. The domain dimensions adopted in the conducted simulations allow for the aerodynamic blade loads to be obtained with negligible error resulting from the assumed boundary conditions. In the case of VAWTs, the fluctuations in aerodynamic loads during each rotation are very significant. Hence, unsteady simulations are necessary, utilising the unsteady Reynolds-averaged Navier-Stokes (URANS) approach. The performed analyses used the ANSYS Fluent 2022 code and the well-known sliding

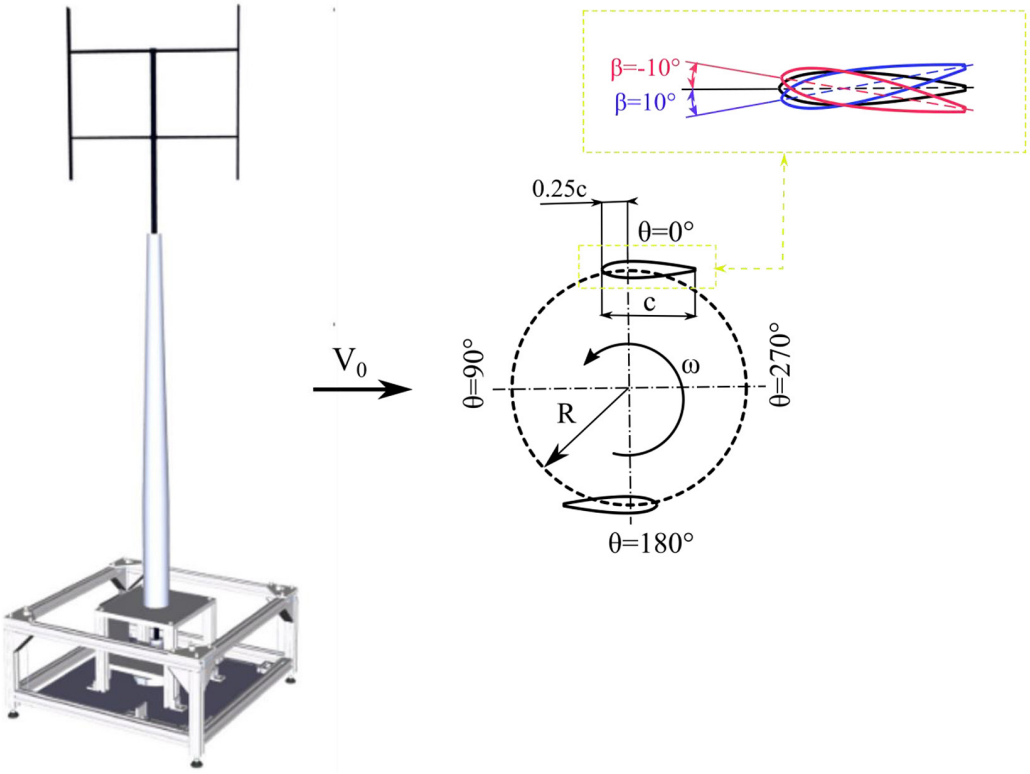

Figure 1. Schematic of the investigated VAWT model. On the left is a conceptual drawing of the laboratory-scale rotor. The figure is taken from [9] with permission. On the right is a 2-D schematic used in numerical computations and the pitch angle convention

mesh technique. However, this technique requires separating the area around the rotor, which will move during the simulation. In the analyzed model, the moving area around the rotor is a circle with a diameter of 1.5 D. Data between both regions is exchanged during calculations via the interface. Applying this condition (interface) may result in a small numerical error at the boundary between areas. However, Bangga et al. [16] demonstrated that the diameter adopted in these studies (1.5 D) is sufficient to minimize numerical error. Figure 2 illustrates the computational domain along with the prescribed boundary conditions. At the domain boundaries, the following boundary conditions are applied: velocity inlet, pressure outlet, and wall (no slip), respectively, at the inlet, outlet, and airfoil edges. In addition, the "symmetry" boundary condition is used on the side edges of the domain, which allows for the same effect as the wall (slip) boundary condition.

The geometric model of the rotor described above was discretized with a control volume mesh. The numerical mesh consists of a structured mesh near the edges of the airfoils and an unstructured mesh in the remaining area. The number of grid points on each airfoil edge was equal to 2400. Rezaeiha et al. [8], who analyzed the sensitivity of the solution to grid density for steady-state calculations of the NACA0015 airfoil at a low Reynolds number, obtained sufficiently accurate results for grid nodes equal to 1600 along the entire airfoil edge. This grid density analyzed by Rezaeiha et al. was subsequently used by them for VAWT simulations. The mesh was not additionally refined near the leading and trailing edges; in other words, the element size along the airfoil edge was uniform. In the normal direction to the airfoil edge, 25 layers of structural mesh were applied. The first layer thickness was 0.00001 m, which ensured a maximum value of the wall y+ parameter < 1.2. However, the average value of this parameter for various rotor angles was approximately 0.8. Maintaining the value of this parameter at the recommended level ≈ 1 is practically impossible in the case of a VAWT rotor calculated using the sliding mesh technique. Moreover, according to the ANSYS Fluent documentation [17], wall y+ < 1.2 values do not produce significant numerical error. Each subsequent layer of the structural mesh was thicker than the previous one, and the growth rate of subsequent layers was 1.1. This value is also

consistent with the recommendations of the ANSYS Fluent documentation. Such a mesh should be sufficient to model all phenomena occurring in the boundary layer during the rotation, such as the laminar-to-turbulent transition and stall effects. At the interface, the same number of grid points was assumed and established to equal 150 in the fixed and moving domains to minimize the numerical error. Therefore, the mesh element size at the interface is 100 times lower than the rotor diameter. The maximum size of unstructured mesh elements in the rotor area (in a circular domain) is 3e-3m. This size is also 100 times lower compared to the rotor diameter. The area in the aerodynamic wake downstream behind the rotor has also been refined. The maximum element size in this area was 60 times lower than the rotor diameter. The area covered by this refined mesh extends 20 D behind the rotor and has a width of 2 D. The modeled mesh effectively captures a broad spectrum of vortex structures present in the rotor and wake regions [18]. The final mesh is depicted in Figure 2, comprising 510.271 elements.

The description above pertains to the geometric and discretized model. The numerical model settings are outlined below. The numerical calculations of the flow around the rotating rotor were conducted using the 2-D URANS approach. The adopted closure model was the 4-equation γ-Re_θ model, known as the Transition SST turbulence model in ANSYS Fluent. To represent the velocity field more accurately in the rotor region and the rotor aerodynamic wake, the Scale Adaptive Simulation (SAS) approach was utilized [19, 20]. The simulations considered air with a constant density of 1.225 kg/m^3 and viscosity of 1.7894e-05 kg/(m·s). A turbulence intensity of 2% was assumed at the inlet [9]. The turbulence scale value at the inlet was not measured; therefore, following Rezaeiha et al. [15], the scale length was assumed to equal the rotor diameter. The coupled scheme was employed for the Pressure-Velocity Coupling method in these investigations. The least squares cell based was also used for spatial discretization and second-order schemes for all computed equations except for the momentum equations, where

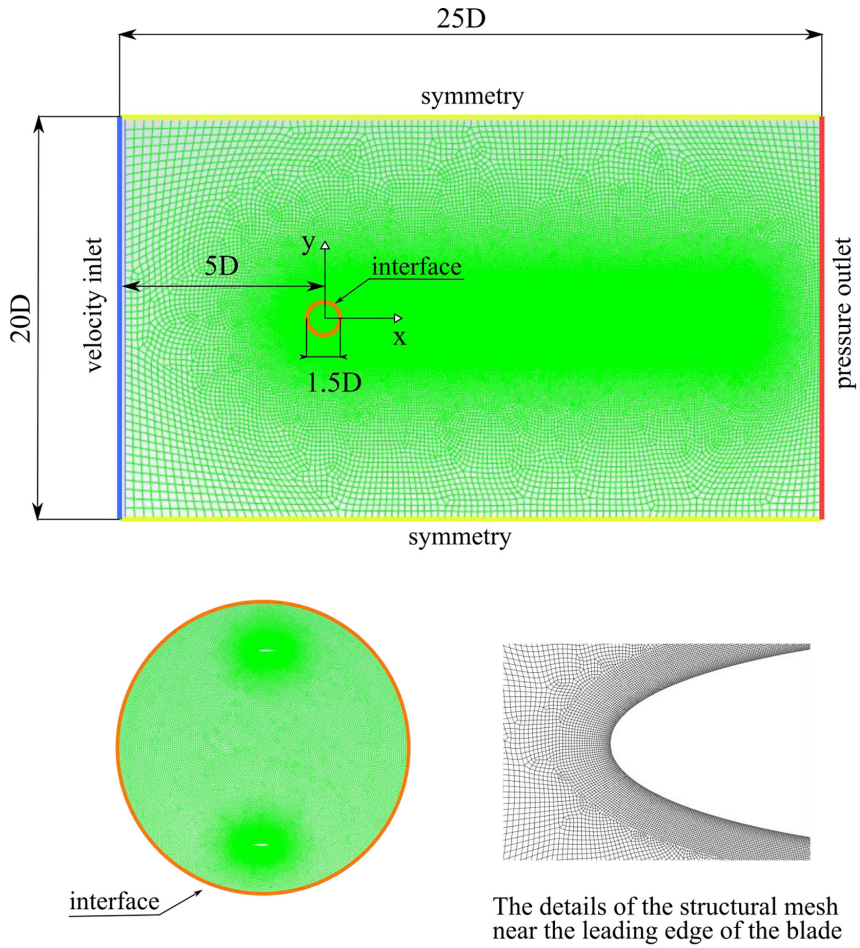

Figure 2. Numerical domain; boundary conditions; mesh

the bounded central differencing was utilized. The convergence criterion for all equations was set to 1e-7. The Courant Number value was left as default, equal to 200. According to [17], in the case of the pressure-based solver and the Coupled scheme, the Courant Number stabilizes the convergence behavior. In these studies, the influence of time step size on the calculated aerodynamic characteristics of the rotor was not analysed. This is, of course, a very significant parameter affecting the accuracy of simulations. However, several credible, independent scientific works have examined this effect depending on various operational parameters of the rotor. Therefore, in this work, the time step size was selected based on the guidelines of Rezaeiha et al. [15] and own experiences [21]. The time step size, Δt, was set in this work to 2.09e-05 seconds, equivalent to an azimuth increment of Δθ = 0.1 deg.

RESULTS AND DISCUSSION

This section presents the characteristics of two components of the aerodynamic force acting on the entire wind turbine rotor: the component parallel to the flow direction, known as thrust, and the lateral force. The obtained loads are then validated against experimental measurements to assess the reliability of the adopted simplified 2-D numerical rotor model. In the next part of this section, aerodynamic loads on the rotor blade are analyzed. The Reynolds-averaged Navier-Stokes simulation was compared with high-fidelity experimental data in this next section of the paper.

Aerodynamic load components

The two components of aerodynamic force, the streamwise (T_x) and lateral (T_y), are given as dimensionless coefficients:

$$C_{T_{x,y}} = \frac{T_{x,y}}{0.5\rho V_0^2 A} \tag{1}$$

where: ρ – air density, V_0 – undisturbed flow velocity, A – the frontal area of the turbine. In the considered rotor $A = D \cdot H$, where H is the rotor height.

Figure 3a depicts the dependence of both components, thrust and lateral, of the aerodynamic force on the number of rotor revolutions. For clarity, only the results for a zero-pitch angle (β = 0 deg) are shown in this graph. In the case of the remaining analyzed pitch angles, the nature of the aerodynamic forces follows a similar pattern. Figure 3a also shows that the influence of initial conditions on these rotor operational parameters (TSR = 2.5) is noticeable only in the first few rotations. Initial conditions, i.e., flow parameters at each control volume at t = 0 s, were assumed to be the same as at the inlet. This effect is visible in the aerodynamic loads corresponding to the first few revolutions in numerical simulations. To eliminate this effect, the number of rotations required to calculate depends on the rotor's operating parameters and geometry. Rogowski [21] also studied the rotor in laboratory-size scale but operating at TSR = 4.5. Rogowski determined that the minimum number of rotations necessary to achieve a power coefficient independent of initial conditions is 15. This result is consistent with the numerical research conducted independently by Rezaeiha [22], who additionally demonstrated that in the case of a rotor with higher solidity, σ, the number of rotations required for simulation slightly increases. The rotor solidity is defined in the case of Darrieus-type rotors as:

$$\sigma = c \cdot N/D \tag{2}$$

where: c – chord length, N – number of turbine blades and D – rotor diameter.

Rezaeiha et al. [22] investigated rotors with solidities of 0.12 and 0.24. In the conducted investigations, this parameter was equal to 0.2. Additionally, Rezaeiha et al. also demonstrated that for a more heavily loaded rotor operating at TSR = 2.5, the influence of initial conditions is significantly reduced. The average power coefficient of the rotor becomes independent of initial conditions after about ten full revolutions. As it can be seen in (Figure 3a), the results of both components of the aerodynamic force differ slightly from each other in each rotor revolution. However, this is the proper behavior of the numerical model and has several reasons. Primarily, the wind turbine rotor operates under significant geometric angles of attack of the rotor blades. The geometric angle of attack, α_g, is determined based on the velocity triangle (Figure 3b) as [23]:

$$\alpha_g = \tan^{-1}\left(\frac{\sin\theta}{\cos\theta + TSR}\right) \tag{3}$$

This model of the geometric angle of attack is, of course, highly simplified. Determining the actual angle of attack is quite challenging. However, there are analytical methods allowing for

estimation of the actual angle of attack based on the velocity field, e.g. [24], indicate that in the upwind part of the rotor (for θ from 0 to 180 deg, see Figure 1), such an approximation is sufficient and enables understanding of certain phenomena. The actual angle of attack differs mainly in the downwind part (for θ from 180 to 360 deg) compared to the geometric angle. It is known that due to the deceleration of the flow velocity by the blades traveling in the upwind part, there can be a significant decrease in the magnitude of the angle of attack depending on the tip speed ratio [9]. Figure 3b shows that at TSR = 2.5, the angle of attack amplitude is significant; in this case, it is as much as 30 degrees.

The second reason for the irregularity of the aerodynamic forces shown in (Figure 3a) is the local blade Reynolds number. The Reynolds number can be approximately estimated using the local geometric angle of attack introduced earlier and the local relative velocity, V_R, given as:

$$V_R = V_0\sqrt{(TSR + \cos\theta)^2 + (\sin\theta)^2} \quad (4)$$

The local Reynolds number is equal to:

$$Re = \frac{V_R \cdot c}{\mu} \quad (5)$$

where: μ – dynamic viscosity of air, c – chord length.

The local Reynolds number is given by equation 3, while its average value is only 21.860. The rotor of the investigated turbine operates in the range of subcritical Reynolds numbers and very large angles of attack.

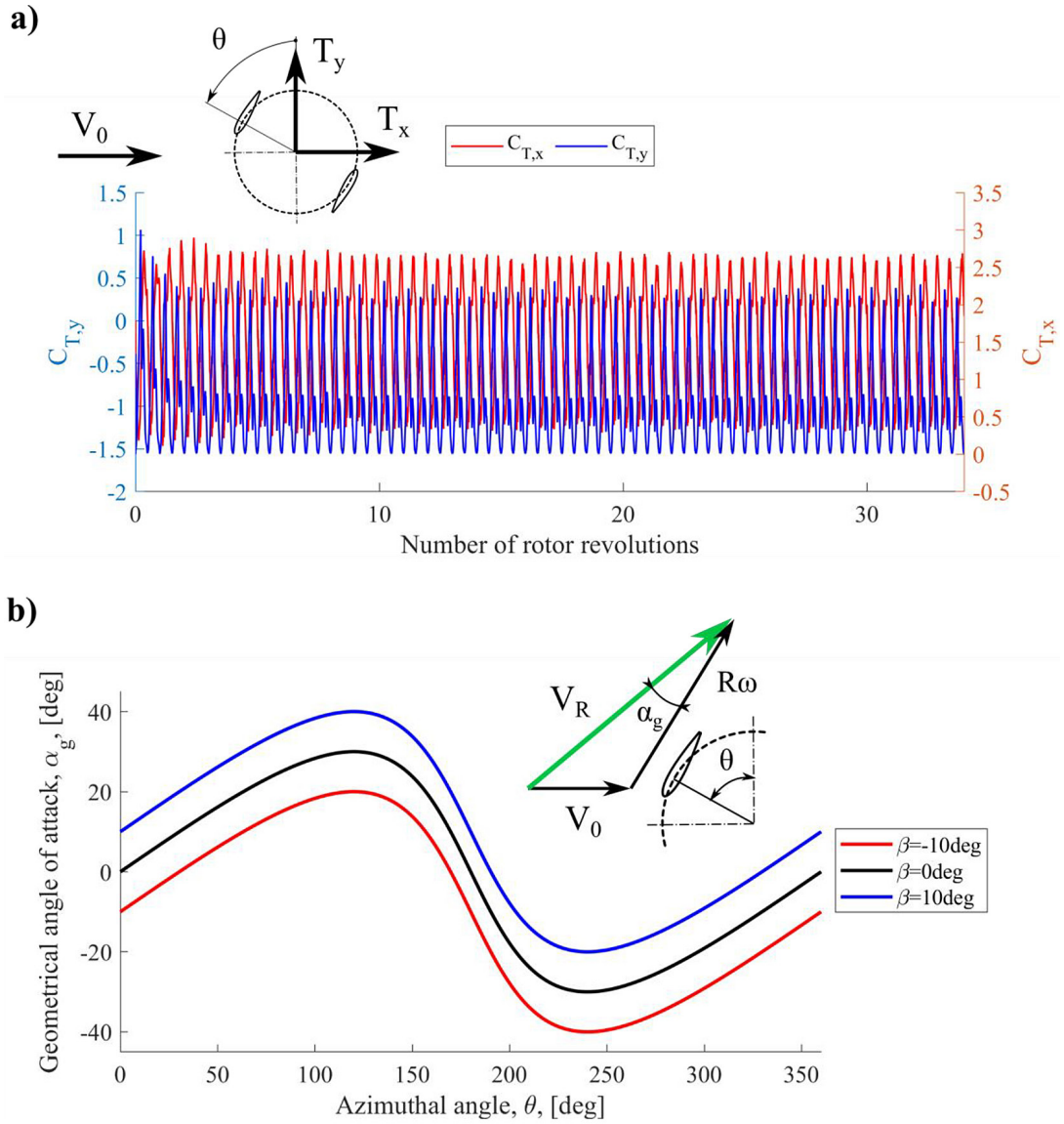

Figure 3. (a) Trust and lateral coefficient, (b) geometric angle of attack for zero-pitch angle configuration

The irregularities shown in (Figure 3a) are also attributed to the turbulence model employed in this study. Using classical one- or two-equation turbulence models such as k-ω or k-ε leads to unrealistic averaging of flow disturbances. Consequently, the wake generated by the blades traveling in the upwind part of the rotor rapidly dissipates, resulting in a regular and repeatable aerodynamic force distribution for individual blades and the entire rotor. Rogowski et al., in their work [20], demonstrated a comparison of aerodynamic loads obtained using classical turbulence models and the Scale Adaptive Simulation approach for a one-bladed Darrieus rotor. Applying this technique allows for capturing much more flow detail and, consequently, a more irregular nature of aerodynamic loads on the blades, which is more physically realistic. This action, however, involves the necessity of averaging the loads over a larger number of rotations than different approaches. Figure 4 shows the dependencies of $C_{T,x}$ and $C_{T,y}$ averaged over one full rotor revolution. These values are presented as a function of the number of revolutions for the last ten calculated rotor revolutions. As it seen in this figure, the average values of the loads differ in each subsequent revolution. However, it should be emphasized that the fluctuations of these average values are small. In the conducted investigation, it was also examined how the components of the aerodynamic force differ when the averaging time is increased. To achieve this, the times corresponding to the averaged rotations ranging from 1 to 10 full rotations of the rotor were investigated. The conducted research has shown that the relative difference of different averaging times compared to the averaging time corresponding to 10 complete rotations is relatively small, not exceeding 3.2% for $C_{T,y}$ and 1% for $C_{T,x}$. Additionally, it was found that an averaging time equal to 5 full rotations is sufficient. The relative errors of $C_{T,y}$ and $C_{T,x}$ components are 1.1% and 0.4%, respectively. Therefore, in all analyses conducted in this paper, the average values of the aerodynamic force components were calculated using the data from the last five rotations of the rotor.

Validation

Table 1 compares the calculated average values of the rotor aerodynamic loads with the values measured by Huang [9]. The obtained results of the $C_{T,x}$ component are slightly overestimated compared to the experimental values, but the nature of the changes for cases $\beta = 0°$ and $\beta = -10°$ is similar. The agreement between the calculated and measured lateral aerodynamic force component is even better. Significant differences were only observed for the case $\beta = 10°$, especially for the $C_{T,x}$ component. These differences can be explained based on the aerodynamic wake patterns behind the wind turbine rotor measured in the

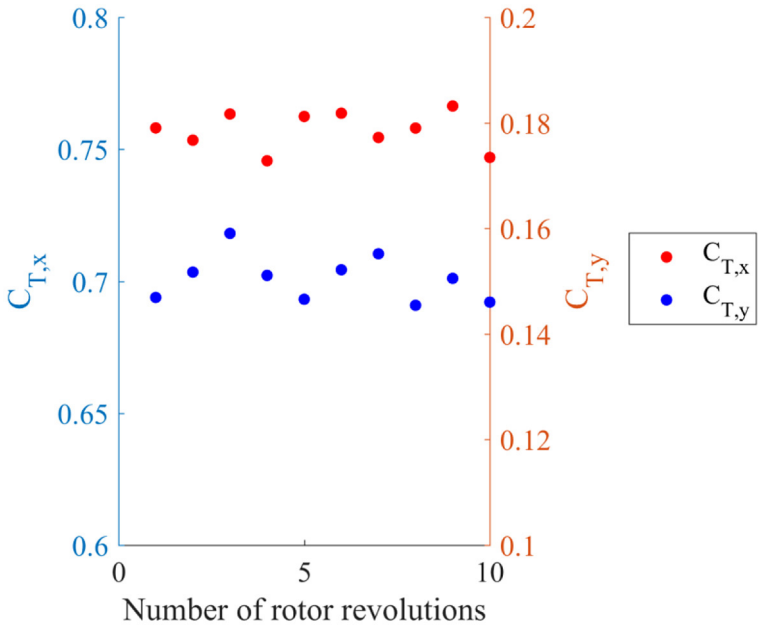

Figure 4. The mean coefficients of the aerodynamic force components for each of the last ten calculated rotations of the rotor

Table 1. Calculated and measured $C_{T,x}$ and $C_{T,y}$

Test case	Trust, $C_{T,x}$			Lateral, $C_{T,y}$		
	Experiment	CFD	Δ%	Experiment	CFD	Δ%
β = –10°	0.60	0.73	21.67	0.09	0.09	0.00
β = 0°	0.65	0.76	16.92	0.14	0.15	7.14
β = 10°	0.81	0.64	-20.99	0.39	0.51	30.17

experiment using the PIV method. In cases β = 0° and β = –10°, the aerodynamic wake is more "filled" in the equatorial plane compared to the case β = 10°. This is due to 3-D effects, which are strongest in this particular case. These effects are impossible to determine using a 2-D numerical approach. Despite the limitations of the applied approach, the largest absolute relative error Δ% is 30% for $C_{T,y}$ and 21% for $C_{T,x}$.

Aerodynamic loads on the rotor blade

The analyses above concerned averaged rotor aerodynamic loads. This part of the paper aimed to determine the aerodynamic load distribution along a single blade. Figures 5a and 5b depict the aerodynamic force components acting on a single rotor blade for the last calculated rotation of the rotor. The aerodynamic loads are presented as dimensionless coefficients for three pitch angles. The coefficients of tangential (C_T) and normal (C_N) aerodynamic forces are given by:

$$C_{T,N} = \frac{T,N}{0.5\rho V_0^2 A} \tag{6}$$

The tangential component of the aerodynamic load is responsible for generating torque, which is the product of the tangential force and the distance from its point of application to the rotor axis. As it is shown in Figure 5b, this force is an order of magnitude smaller than the normal component. Moreover, as it can be seen from this figure, a large portion of all displayed C_T characteristics has a negative value. The average C_T values for all analyzed pitch angles are negative and close to zero. Negative values of the tangential force indicate that a rotor with such a configuration must be powered to maintain the desired operational conditions. The normal component (Figure 5a) is slightly shifted for angles β = –10° and β = 10° compared to the β = 0°. This is due to the shift of the local attack angle at the introduced pitch angles. Therefore, such behavior of the characteristics proves the correct qualitative functioning of the simplified numerical model. Numerous fluctuations of the components, on the other hand, indicate a very complex nature of the flow in the regime of deep dynamic stall.

Velocity deficit profiles

In this part of the paper, the Reynolds-averaged Navier-Stokes simulation was compared

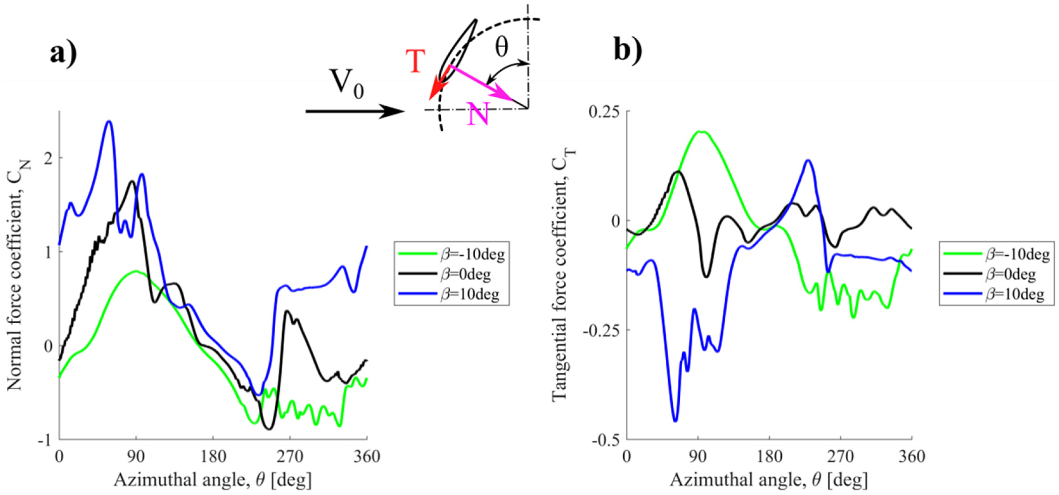

Figure 5. Aerodynamic blade load coefficients at three pitch angles: (a) normal components, (b) tangential components

with high-fidelity experimental data and with the actuator line model (ALM) results by Huang [9]. Figure 6 compares the velocity deficit profiles for two cases: $\beta = 0°$ and $\beta = 10°$, where $\Delta u/V_0 = 1 - u/V_0$, where u represents a local air velocity component parallel to the undisturbed flow velocity. The results presented in this figure have been averaged over one full rotor revolution. In this case, the additional influence of averaging time on wake velocity characteristics was not tested. However, as it can be observed in (Fig. 6), the simplified 2-D model with the SAS approach reasonably covers the velocity profiles for the $\beta = 0°$ case even at a distance of 10D downstream from the rotor. It can be further seen from Fig. 6 that the SAS approach provides more details about the flow itself. Unfortunately, the wake predictions for the most heavily loaded rotor ($\beta = 10°$) are significantly worse up to 5D behind the rotor. In this case, the reduced 2-D model shows significant differences in velocity deficit profiles.

As it is shown in (Figure 6), the ALM + RANS approach provides significantly higher fidelity compared to the CFD approach for the $\beta = 10°$ case. The ALM approach incorporates a

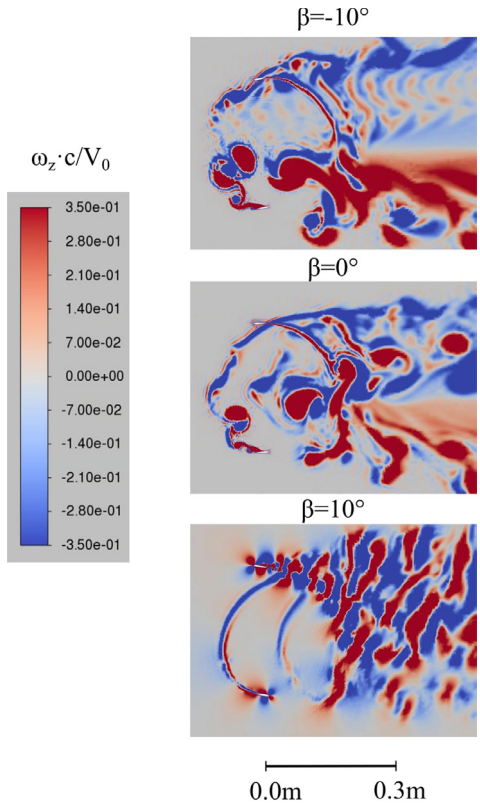

Figure 7. Contours of normalized z-vorticity in the rotor area at three pitch angles

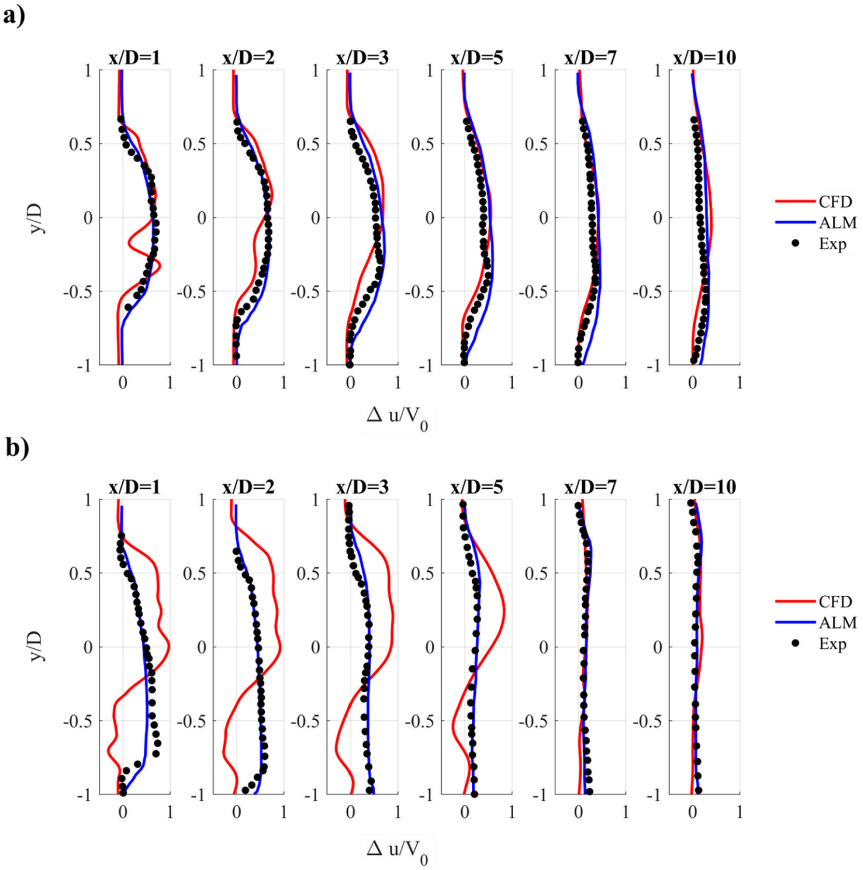

Figure 6. Velocity deficit profiles for (a) $\beta = 0°$, (b) $\beta = 10°$

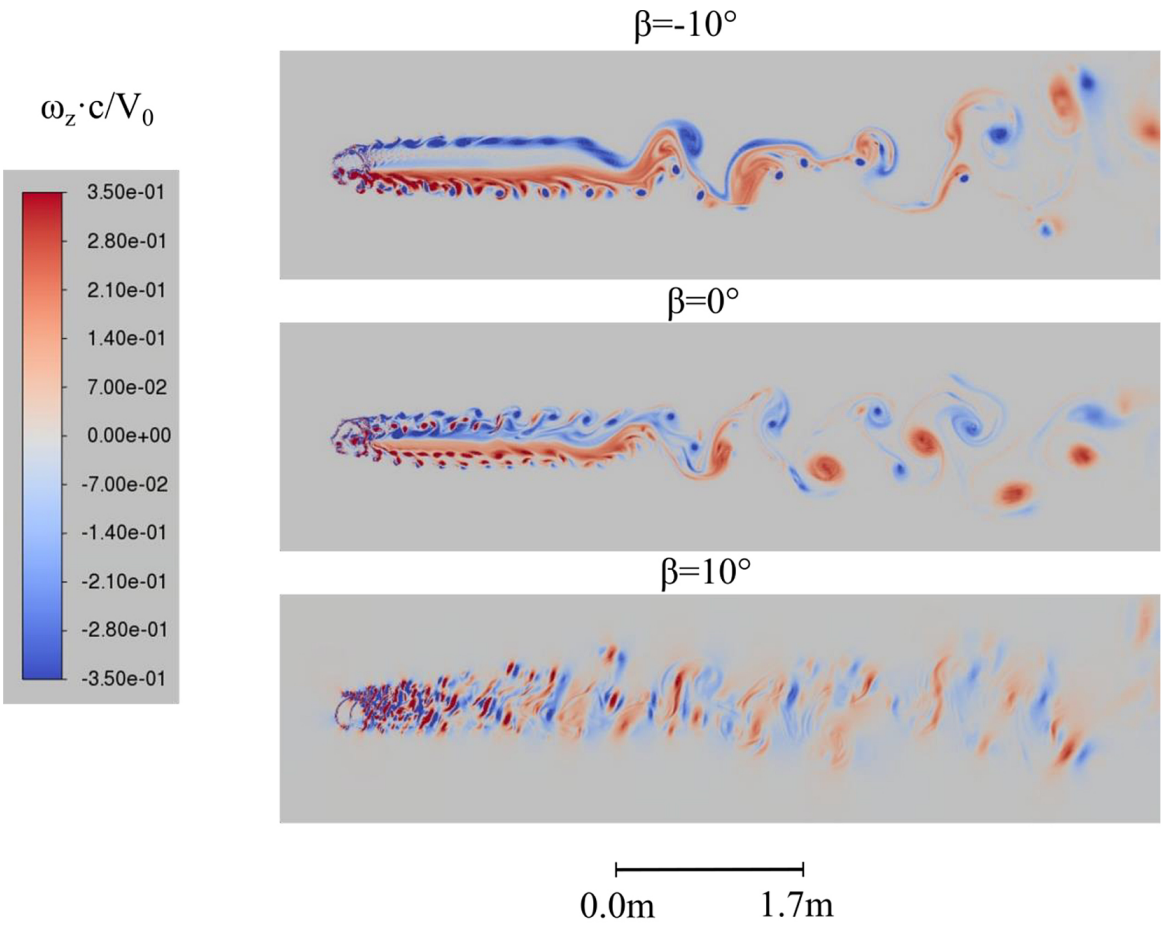

Figure 8. Contours of normalized z-vorticity in the wake of the rotor at three pitch angles

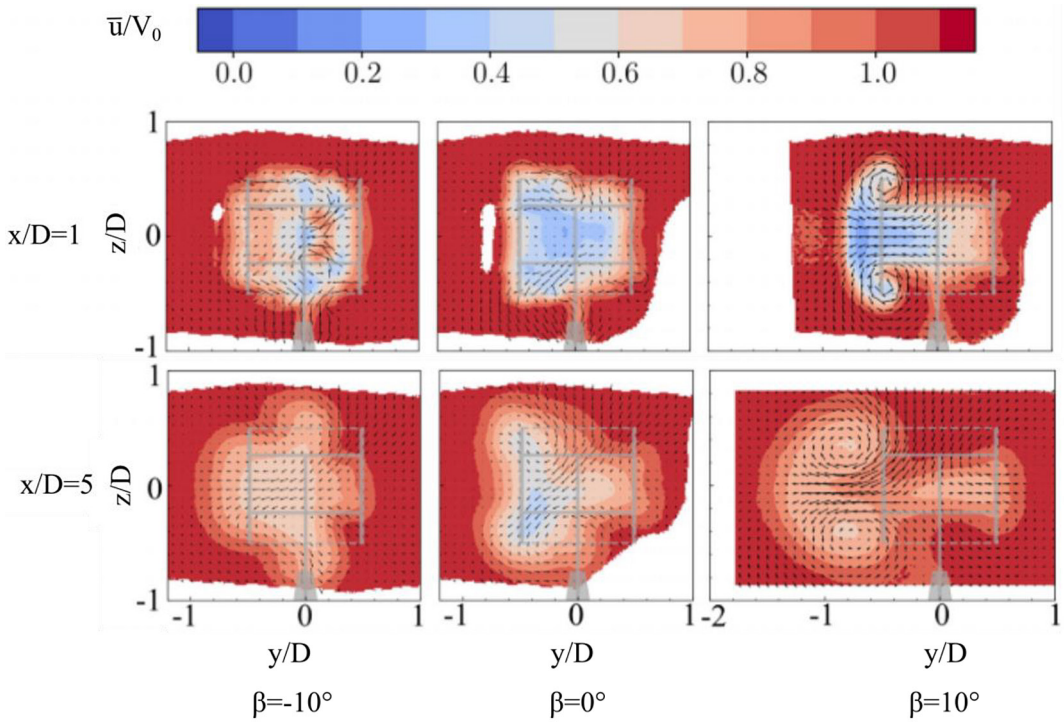

Figure 9. Contours of streamwise velocity with in-plane velocity vectors for the VAWT at three pitch angles and at two positions behind the rotor. The photos come from Huang's doctoral dissertation [25]. The authors of this paper have the permission to publish them

three-dimensional rotor model, while to determine the velocity field in the rotor region, the URANS approach with the k-ε turbulence model was employed [9].

Figures 7 and 8 depict contours of normalized vorticity ω_z for three analyzed pitch angles. In 2-D flow, the velocity lacks a z-component, and the vorticity vector is parallel to the rotor axis. The red and blue colors correspond to opposite directions of the vorticity vector. Contour maps were prepared on two scales to illustrate differences in flow structure around the rotor and far downstream. Both figures compare instantaneous vorticity fields for the same azimuthal position. Calculations were performed for 40 complete rotor revolutions to ensure fully developed vorticity fields. The results clearly demonstrate a similar flow character for cases of $\beta = 0°$ and $\beta = –10°$, and a completely different character for the case of $\beta = 10°$.

CONCLUSIONS

The main aim of this paper was to validate a reduced numerical model of a vertical-axis wind turbine based on high-fidelity experimental data developed at TU Delft [9]. The model was simplified by replacing the three-dimensional rotor with a two-dimensional model. The primary numerical tool employed was the Scale Adaptive Simulation approach with the Transition SST turbulence model. The results obtained allowed drawing the following conclusions:

The operating conditions and geometry of the rotor are extreme. Flow in the rotor region is highly complex, and the blades operate under conditions of deep dynamic detachment.

Significant differences in the aerodynamic wake compared to the experiment, especially for the case of $\beta = 10°$, are mainly due to 3-D phenomena. The 2-D model cannot account for changes in velocity and pressure in the axial direction, as well as the interactions between the blades and the blade tips.

Introducing a significant positive pitch angle increases the local angle of attack and normal blade loading, resulting in the formation of strong trailing edge vortices that significantly modify the two-dimensional flow. Figure 9 depicts the time-averaged streamwise velocity contours and in-plane velocity vectors of the laboratory-scale VAWT operating at various pitch angles and in different positions behind the rotor. These findings were obtained through stereo-PIV measurements.

As long as the trailing edge vortices are small to moderate, the aerodynamic wake is more "filled" and uniform. Under such conditions, the reduced approach yields significantly better results. A pitch angle of 10 degrees significantly alters the lateral force and, therefore, modifies the wake geometry. A positive pitch angle results in significant blade work under conditions of dramatic detachment but also significantly modifies the flow in the rotor wake. This effect can be utilized in designing a wind farm with such rotors for passive control of wake geometry. Deterioration of the aerodynamic properties of the upstream rotor may enhance the performance of the wind turbine array.

As it is shown in this paper, the 2-D CFD approach fails in the case of the most heavily loaded rotor. However, the 2-D model is attractive due to its low computational cost, even with the current level of computerization. Therefore, to completely rule out this approach in studies of such cases, it is necessary to examine one more significant aspect. Specifically, the impact of the rotor aspect ratio (AR), which is the ratio of the rotor height to its diameter, on the geometry of the aerodynamic wake needs to be analyzed. Huang studied this effect using a two-bladed VAWT configuration based on experimental research from Delft. The examined rotor had a diameter of 1 m and a blade chord length of 0.06 m. The aerodynamics of this rotor were analyzed at TSR = 4.5. Studies conducted using the ALM technique for ARs ranging from 1 to 10 showed that the thrust coefficient of this rotor increased from 0.75 for AR = 1 to 0.91 for AR = 10. This suggests that the width of the aerodynamic wake should increase with AR. However, Huang's studies focused only on the case of $\beta = 0°$. Therefore, a hypothesis can be proposed: in the case where $\beta > 0°$ (or even $\beta >> 0°$) and AR is sufficiently large, the 2-D CFD model will provide more physical results. This hypothesis, however, requires appropriate experimental and numerical analyses.

Acknowledgements

Research was funded by POB Energy of Warsaw University of Technology within the Excellence Initiative: Research University (IDUB) programme (Grant No. 1820/355/Z01/POB7/2021). This research was also conducted

with the assistance of the Interdisciplinary Centre for Mathematical and Computational Modelling (ICM) at the University of Warsaw under computational allocations no. G93-1588 and G92-1487. I would like to express my heartfelt gratitude to Mr. Eng. Tomasz Szuster, a retired academic teacher from the Warsaw University of Technology, for his invaluable support and guidance.

REFERENCES

1. Kumar R., Raahemifar K., Fung A.S. A critical review of vertical axis wind turbines for urban applications. Renewable and Sustainable Energy Reviews. 2018, 89, 281–91. DOI: 10.1016/j.rser.2018.03.033.
2. Bianchini A., Ferrara G., Ferrari L. Pitch optimization in small-size darrieus wind turbines. Energy Procedia. 2015, 81, 122–32. DOI: 10.1016/j.egypro.2015.12.067.
3. Du L., Ingram G., Dominy R.G. A review of H-Darrieus wind turbine aerodynamic research. Proceedings of the Institution of Mechanical Engineers, Part C: Journal of Mechanical Engineering Science. 2019, 233(23–24), 7590–616. DOI: 10.1177/0954406219885962.
4. Amet E., Maître T., Pellone C., Achard J.L. 2D Numerical simulations of blade-vortex interaction in a darrieus turbine. Journal of Fluids Engineering. 2009, 131(111103). DOI: 10.1115/1.4000258.
5. Rezaeiha A., Montazeri H., Blocken B. Characterization of aerodynamic performance of vertical axis wind turbines: Impact of operational parameters. Energy Conversion and Management. 2018, 169, 45–77. DOI: 10.1016/j.enconman.2018.05.042.
6. Fiedler A.J., Tullis S. Blade offset and pitch effects on a high solidity vertical axis wind turbine. Wind Engineering. 2009, 33(3), 237–46. DOI: 10.1260/030952409789140955.
7. Elkhoury M., Kiwata T., Aoun E. Experimental and numerical investigation of a three-dimensional vertical-axis wind turbine with variable-pitch. Journal of Wind Engineering and Industrial Aerodynamics. 2015, 139, 111–23. DOI: 10.1016/j.jweia.2015.01.004.
8. Rezaeiha A., Kalkman I., Blocken B. Effect of pitch angle on power performance and aerodynamics of a vertical axis wind turbine. Applied Energy. 2017, 197, 132–50. DOI: 10.1016/j.apenergy.2017.03.128.
9. Huang M., Sciacchitano A., Ferreira C. On the wake deflection of vertical axis wind turbines by pitched blades. Wind Energy. 2023, 26(4), 365–87. DOI: 10.1002/we.2803.
10. Szczerba Z., Szczerba P., Szczerba K., Szumski M., Pytel K. Wind tunnel experimental study on the efficiency of vertical-axis wind turbines via analysis of blade pitch angle influence. Energies. 2023, 16(13), 4903. DOI: 10.3390/en16134903.
11. Elsakka M.M., Ingham D.B., Ma L., Pourkashanian M., Moustafa G.H., Elhenawy Y. Response surface optimisation of vertical axis wind turbine at low wind speeds. Energy Reports. 2022, 8, 10868–80. DOI: 10.1016/j.egyr.2022.08.222.
12. Menter F.R., Langtry, R.B., Likki, S.R., Suzen, Y.B., Huang, P.G., Völker, S.A. Correlation-based transition model using local variables: Part I—model formulation. J. Turbomach. 2006, 128, 413–422. DOI: 10.1115/1.2184352.
13. Michna J., Rogowski K. Numerical study of the effect of the reynolds number and the turbulence intensity on the performance of the NACA 0018 airfoil at the low reynolds number regime. Processes. 2022, 10, 1004. DOI: 10.3390/pr10051004.
14. Huang M., Ferreira C., Sciacchitano A., Scarano F. Experimental comparison of the wake of a vertical axis wind turbine and planar actuator surfaces. J. Phys. Conf. Ser. 2020, 1618, 052063. DOI: 10.1088/1742-6596/1618/5/052063.
15. Rezaeiha A., Kalkman I., Blocken B. CFD simulation of a vertical axis wind turbine operating at a moderate tip speed ratio: Guidelines for minimum domain size and azimuthal increment. Renew. Energy 2017. 107, 373–385. DOI: 10.1016/j.renene.2017.02.006.
16. Bangga G., Hutomo G., Wiranegara R., Sasongko H. Numerical study on a single bladed vertical axis wind turbine under dynamic stall. J. Mech. Sci. Technol. 2017. 31(1), 261–267. DOI: 10.1007/s12206-016-1228-9.
17. Ansys® Fluent Release 2022, ANSYS, Inc.
18. Mendoza V., Bachant P., Ferreira C., Goude A. Near-wake flow simulation of a vertical axis turbine using an actuator line model. Wind Energy 2019. 22, 171–188. DOI: 10.1002/we.2277.
19. Rezaeiha A., Montazeri H., Blocken B. CFD analysis of dynamic stall on vertical axis wind turbines using Scale-Adaptive Simulation (SAS): Comparison against URANS and hybrid RANS/LES. Energy Convers. Manag. 2019. 196, 1282–1298. DOI: 10.1016/j.enconman.2019.06.081.
20. Rogowski K., Hansen M., Maroński., Lichota P. Scale adaptive simulation model for the darrieus wind turbine. J. Phys. Conf. Ser. 2016, 753, 022050. DOI: 10.1088/1742-6596/753/2/022050.
21. Rogowski K. CFD computation of the H-Darrieus wind turbine—The impact of the rotating shaft on the rotor performance. Energies 2019. 12(13), 2506. DOI: 10.3390/en12132506.
22. Rezaeiha A., Montazeri H., Blocken B. Towards accurate CFD simulations of vertical axis wind

turbines at different tip speed ratios and solidities: Guidelines for azimuthal increment, domain size and convergence. Energy Convers. Manag. 2018. 156, 301–316. DOI: 10.1016/j.enconman.2017.11.026.

23. Rogowski K., Maroński R., Piechna J. Numerical analysis of a small-size vertical-axis wind turbine performance and averaged flow parameters around the rotor. Arch. Mech. Eng. 2017, 64(2), 205–218. DOI: 10.1515/meceng-2017-0013.
24. Mendoza V., Bachant P., Wosnik M., Goude A. Validation of an Actuator line model coupled to a dynamic stall model for pitching motions characteristic to vertical axis turbines. J. Phys. Conf. Ser. 2016, 753, 022043. DOI: 0.1088/1742-6596/753/2/022043.
25. Huang M. Wake and wind farm aerodynamics of vertical axis wind turbines. Doctoral dissertation, Technische Universiteit Delft, 2023. DOI: 10.4233/uuid:14619578-e44f-45bb-a213-a9d179a54264.